

This item is the archived peer-reviewed author-version of:

Analysis of hyperspectral images for detection of drought stress and recovery in maize plants in a high-throughput phenotyping platform

Reference:

Moh Asaari Mohd Shahrime, Mertens Stien, Dhondt Stijn, Inzé Dirk, Wuyts Nathalie, Scheunders Paul, Moh Asaari Mohd Shahrime.- Analysis of hyperspectral images for detection of drought stress and recovery in maize plants in a high-throughput phenotyping platform
Computers and electronics in agriculture - ISSN 0168-1699 - 162(2019), p. 749-758
Full text (Publisher's DOI): <https://doi.org/10.1016/J.COMPAG.2019.05.018>
To cite this reference: <https://hdl.handle.net/10067/1605110151162165141>

1 Analysis of hyperspectral images for detection of drought stress and
2 recovery in maize plants in a high-throughput phenotyping platform

3 Mohd Shahrimie Mohd Asaari^{1,4*}, Stien Mertens^{2,3}, Stijn Dhondt^{2,3}, Dirk Inzé^{2,3}, Nathalie
4 Wuyts^{2,3}, Paul Scheunders¹

5 ¹*Imec-Vision Lab, University of Antwerp, Belgium*

6 ²*Ghent University, Department of Plant Biotechnology and Bioinformatics, Ghent, Belgium*

7 ³*VIB Center for Plant Systems Biology, Ghent, Belgium*

8 ⁴*School of Electrical and Electronic Engineering, Universiti Sains Malaysia, Engineering Campus, Nibong
9 Tebal, Penang, Malaysia*

10 **Abstract**

11 The study of physiological processes resulting from water-limited conditions in crops is
12 essential for the selection of drought-tolerant genotypes and the functional analysis of related
13 genes. A promising, non-invasive technique for plant trait analysis is close-range hyperspec-
14 tral imaging (HSI), which has great potential for the early detection of plant responses to
15 water deficit stress. In this work, a data analysis method is described that, unlike vege-
16 tation indices, the present method applies spectral similarity on selected bands with high
17 discriminative information, while requiring a careful treatment of uninformative illumination
18 effects. The latter issue is solved by a standard normal variate (SNV) normalisation that
19 removes linear effects and a supervised clustering approach to remove pixels that exhibit
20 nonlinear multiple scattering effects. On the remaining pixels, the stress-related dynamics
21 is quantified by a spectral analysis procedure that involves a supervised band selection pro-
22 cedure and a spectral similarity measure against well-watered control plants. The proposed
23 method was validated by a large-scale study of water-stress and recovery of maize plants in a
24 high-throughput plant phenotyping platform. The results showed that the analysis method
25 allows for an early detection of drought stress responses and of recovery effects shortly after
26 re-watering.

27 *Keywords:* Close-range hyperspectral imaging, high-throughput plant phenotyping,
28 clustering, spectral similarity measure, drought stress

29 1. Introduction

30 Imaging techniques have improved the precision and throughput of plant phenotyping,
31 and now become a new frontier in phenotypic trait measurement. Current phenotyping plat-
32 forms include a variety of imaging modalities to obtain high-throughput, non-destructive
33 phenotype data for quantitative assessment of structural and functional plant traits. Plant
34 trait assessment in high-throughput plant phenotyping platforms (HTPP) has recently been
35 studied using close-range hyperspectral imaging (HSI) as a promising non-invasive tool (Ge
36 et al., 2016; Mishra et al., 2017). In particular, HSI has been applied for the assessment of
37 plant responses to biotic and abiotic stress conditions, such as fungal infection, water and
38 nutrient deficits. During the stress development, a number of physiological and biochemical
39 responses happen in plants, including modifications in the functioning of the photosynthetic
40 apparatus, plant organ, water content, leaf surface and internal structure. These modifi-
41 cations alter the leaf optical properties (Sun et al., 2018a) that can be measured by HSI.
42 Recent advances in this field encourage studies on plant responses to drought stress, and on
43 the plant's capability to adapt and recover from this stress. Such studies are crucial for the
44 further improvement of crop drought-tolerance in breeding programs.

45 A common approach for plant trait estimation based on HSI is to utilize vegetation indices
46 (VIs), defined as ratios or linear combinations of reflectances at a few single wavelengths.
47 One advantage of VIs is that they minimize the possible influence of scale factors, including
48 slope effects and variations in illumination conditions (Jay et al., 2017). VIs usually focus
49 on very specific biological traits and processes in plants (Heiskanen et al., 2013; Katsoulas
50 et al., 2016; Ihuoma and Madramootoo, 2017), whereas the complex physiological effects of
51 drought stress alter the reflectance in many different wavelength regions. Thus, VIs may
52 discard significant information leading to a decrease in the discrimination accuracy (Römer
53 et al., 2012).

54 Another widely used method for retrieving vegetation characteristics from reflectance
55 data is the inversion of radiative transfer models (RTM). In RTM inversion, model param-

eters such as chlorophyll concentration, water content, dry matter, and canopy structures are retrieved using look-up-tables and optimization techniques (Sun et al., 2018b). A common challenge of these methods is their ill-posedness (Jacquemoud et al., 2009), as various combinations of vegetation parameters may correspond to almost similar spectra. Moreover, this method does not apply well to close-range settings because the physically-based leaf or canopy RTMs are difficult to adapt to the specific close-range illumination problems (Jay et al., 2016).

Data-driven machine learning regression algorithms provide a third way to retrieve plant biophysical variables from the reflectance spectrum (Verrelst et al., 2015; Rapaport et al., 2015). Regression analysis reveals statistical correlations between the spectral variables and biological information. Typically, a flexible learning model is inferred from a training dataset by optimizing the estimation error of the extracted variables. As they implicitly derive the underlying model distribution from a given dataset, these methods are very flexible. However, they cannot be applied if the required output variables for training the model are not available.

In this work, an alternative data-driven method is proposed. To eliminate scaling effects from leaf orientations and specific alignment of the imaging system in close-range settings, a standard normal variate (SNV) normalisation is applied first. To filter out noninformative nonlinear variability induced by multiple scattering and shading in more complex canopy structures, a supervised clustering procedure is proposed and clusters of spectra associated to shadowed and partially occluded areas were discarded. To quantify the dynamics of the water-deficit stress response of a plant, it was characterized by the average SNV spectrum from the retained clusters. An Euclidean distance function was then applied to discriminate stressed from well-watered plants. To optimize the discrimination, a supervised band selection procedure was applied to extract a small subset of top-scoring variables with high class separability. The proposed methodology was validated by a large scale experiment in a HTPP that monitored maize plants during their entire vegetative development period. Six different groups of test plants were monitored: well-watered control plants, and five groups of plants undergoing different water-deficit stress conditions, for which we analysed their

85 response to the drought stress and their recovery after re-watering.

86 **2. Materials and methods**

87 *2.1. Data acquisition*

88 A batch of maize plants was grown in PHENOVISION, the HTPP infrastructure located
89 at VIB, Ghent, Belgium. The plants were divided into six groups undergoing different water
90 irrigation strategy (Figure 1). All treatments started at the seedling level.

- 91 • Group WW (Figure 1 (a)): the well-watered treatment. Seven plants were irrigated
92 with sufficient water to keep the soil water content at the optimal level of 2.4 g H₂O/g
93 dry soil throughout the entire plant developmental period.
- 94 • Group PD-RW1 (Figure 1 (b)): the progressive drought with re-watering 7 days after
95 the V5-stage treatment. Seven plants received a WW treatment from the beginning
96 (seedling) until they reached the V5-stage (five leaves developed). At the V5-stage,
97 the plants were not irrigated for seven days (at that time they reach V6 or V7), after
98 which they were re-watered at V6-stage (six leaves developed) with a low amount of
99 water to maintain the soil water content at a deficit level of 1.4 g H₂O/g dry soil until
100 the end of the developmental period.
- 101 • Group PD-RW2 (Figure 1 (c)): the progressive drought with re-watering 7 days after
102 V5-stage and at V12-stage treatment. Seven plants received the PD-RW1 treatment up
103 to V12 vegetation stage (twelve leaves developed). From V12-stage onward, the plants
104 were irrigated with the WW treatment until the end of the developmental period.
- 105 • Group SD (Figure 1 (d)): the severe drought treatment. Four plants were irrigated
106 with a deficit soil water content of 1.4 g H₂O/g dry soil throughout the developmental
107 period.
- 108 • Group SD-RW1 (Figure 1 (e)): the severe drought with re-watering at the V7-stage.
109 Six plants received the SD treatment from the beginning until they reached the V7-

110 stage (seven leaves developed). From this stage onward, the plants were irrigated
111 according to the WW treatment until the end of the developmental period.

112 • Group SD-RW2 (Figure 1 (f)): the severe drought with re-watering in the V12-stage
113 treatment. Seven plants received the SD treatment from the beginning until they
114 reached the V12-stage after which they were irrigated according to the WW treatment
115 until the end of the developmental period.

116 From all plants involved, hyperspectral images were acquired daily during 50 days from
117 growth stage V2 (two leaves developed), about 2 weeks after the start of the water treat-
118 ments. A line scan push-broom VNIR-HS camera (ImSpector V10E, Spectral Imaging,
119 Oulu, Finland) was used to capture the hyperspectral images. The completed acquisition
120 process produced 350 hyperspectral images for each WW, PD-RW1, PD-RW2 and SD-RW2
121 treatment, 300 images for SD-RW1 and 200 images for SD treatment, which resulted in a
122 total of 1900 images. The acquired images had 510×328 pixels and an average spectral
123 sampling of 3.1 nm which corresponds to 194 bands ranging between 400-1000 nm.

124 All images were radiometrically calibrated by subtracting a dark frame and reflectance
125 was calculated relative to a white reference. Because of high noise levels below 500 nm and
126 above 850 nm (Figure 2), the images were limited to 111 spectral bands in the range 500-850
127 nm for further data processing. The levels Gaussian noise present in the spectrum were first
128 quantified (see Table 1) using the Generalized Cross Validation (GCV) score (Garcia, 2010).
129 The plant pixels were then segmented from the background using the normalized difference
130 vegetation index (NDVI). All pixels with a NDVI higher than 0.3 were segmented as plant
131 pixels (see Figure 3).

132 All plants were imaged in indoor environment inside a closed cabin. The imaging cabin
133 is illuminated with halogen lamps homogeneously distributed in a 2-dimensional plane of
134 the field of view of the HS camera. Although the illumination is well controlled, spectral
135 variability still exist due the physical phenomena of light reflection. In particular, the
136 high spatial resolution of HSI in close-range sensing used here makes the recorded signal
137 very sensitive to specific alignment of the imaging system and the non-solid architecture of

138 the plant. This sensitivity increase further in the whole-plant screening scenarios, where
 139 the crops are susceptible to complex plant geometry. Assuming that the leaf surface is a
 140 Lambertian, the fraction of the leaf reflectance received by the sensor is largely affected
 141 by the inclination of the leaf towards the light source and the distance towards the sensor.
 142 These physical effects can be explained by the Lambert's cosine law and the inverse square
 143 law, which describe that these variabilities induce multiplicative and additive effects on
 144 the reflectance spectra. This induces high uninformative variability in the recorded signals
 145 which overlay the subtle effects of the biological traits. Since these effects are linear, a linear
 146 pre-treatment technique, the Standard Normal Variate (SNV) was applied (Asaari et al.,
 147 2018) to reduce these nuisance variabilities.

Table 1: Gaussian noise estimation on the full and several sub-regions of the obtained spectrum in Figure 2.
 The estimated variance of this noise are estimated based on GCV score (Garcia, 2010). Lower GCV score
 indicates the noise level is low.

Wavelength Region	Estimated Noise Variance (GCV score)
400 nm - 1000 nm	4.560×10^{-2}
400 nm - 500 nm	5.677×10^{-1}
400 nm - 850 nm	7.320×10^{-2}
500 nm - 850 nm	3.416×10^{-5}
500 nm - 980 nm	1.434×10^{-4}
500 nm - 1000 nm	3.890×10^{-4}
850 nm - 1000 nm	1.600×10^{-3}

148 2.2. Clustering

149 The SNV normalization method only accounts for linear scaling effects. In larger plants
 150 with a more complex canopy structure, partially occluded leaves, shadowing and multiple
 151 reflections at the leaf edges cause unwanted nonlinear variability. To remove this variability,
 152 a clustering procedure to discard these regions is proposed.

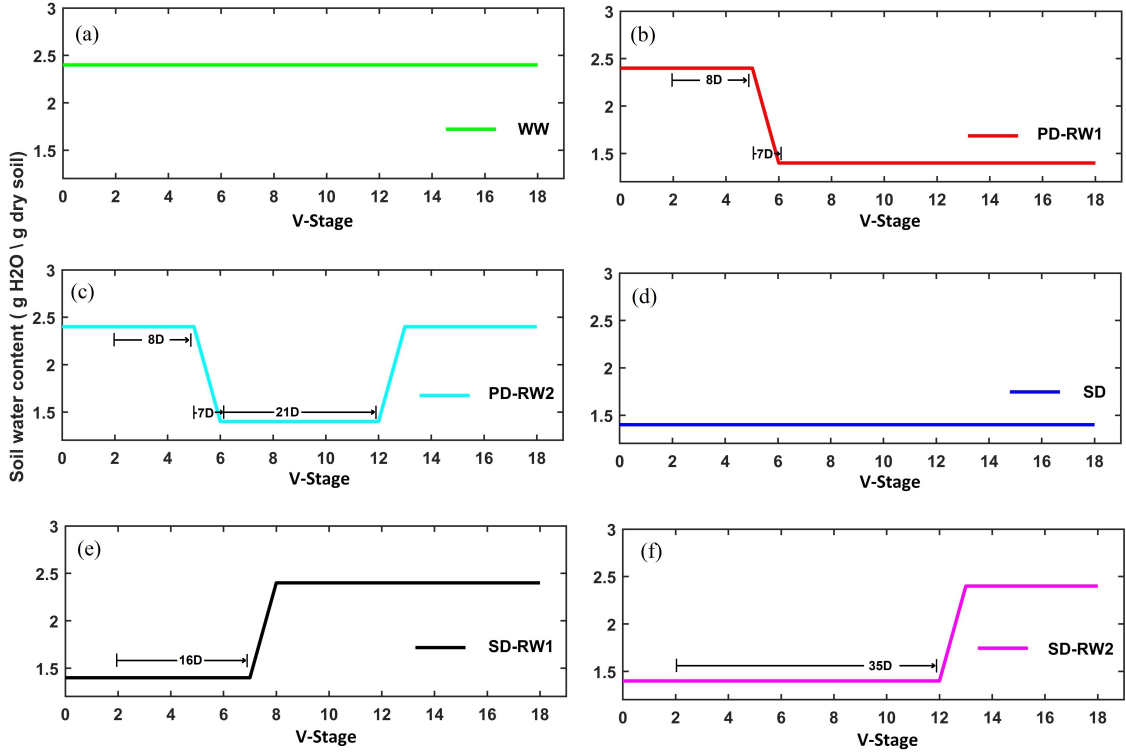


Figure 1: Six different irrigation strategies applied to maize plants, showing the level of soil water content over the entire vegetative developmental period at different V-stages, indicating the number of developed plant leaves and the day at which the plants reach a particular V-stage. (a) well-watered treatment (WW), (b) progressive drought with re-watering 7 days after V5-stage treatment (PD-RW1), (c) progressive drought with re-watering 7 days at a water deficit levels after V5-stage and in the V12-stage treatment at a WW level (PD-RW2), (d) severe drought treatment (SD), (e) severe drought with re-watering in the V7-stage at a WW level (SD-RW1) and (f) severe drought with re-watering in the V12-stage at a WW level (SD-RW2).

153 Typically, unsupervised clustering such as the k -means clustering algorithm can be ap-
 154 plied (Asaari et al., 2018; Behmann et al., 2014). In the proposed experiments, tens of
 155 millions of spectra are involved. The large-scale data streams in HTPP systems pose com-
 156 putational challenges as the system memory may become saturated. Therefore, in this
 157 work, a different clustering strategy is proposed: a supervised method, which combines the
 158 Support Vector Machine (SVM) classifier with the k -means clustering algorithm (Li et al.,
 159 2004). Since it is a supervised algorithm, it requires labeled instances for training the classi-
 160 fier. To avoid time-consuming manual labeling, unsupervised labeling is performed to create

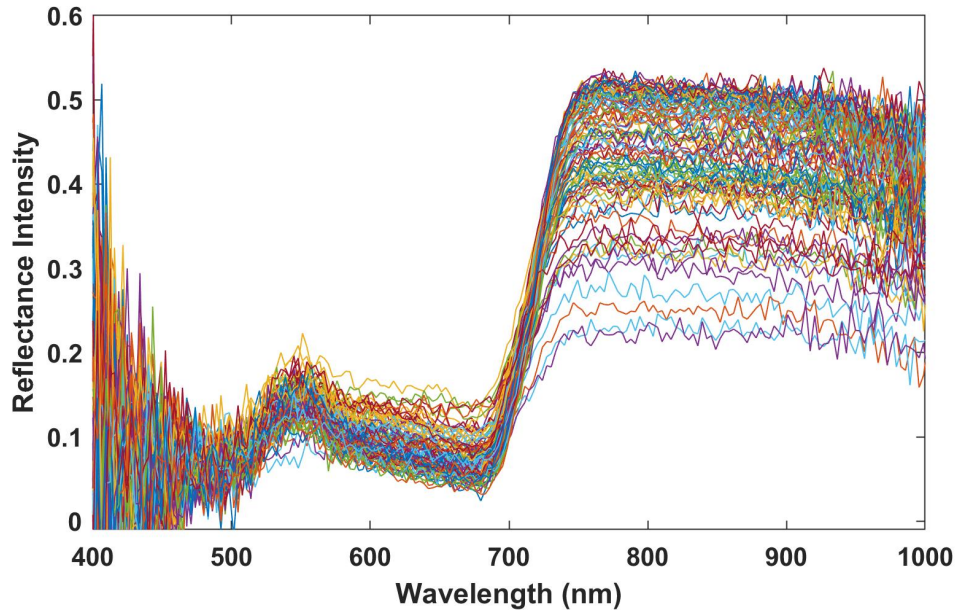


Figure 2: The obtained reflectance spectra covering the spectrum region between 400 nm to 1000 nm. The presented spectrum are those selected from the plant pixels. The spectrum show high noise levels occur at wavelength region below 500 nm and above 850 nm. In order to avoid impairments from noisy data, a reduced spectrum from 500 nm to 850 nm was used. The noise level were quantified using the GCV score matrix (see Table 1).

161 representative spectra for different groups of pixels.

162 In first instance, k -means clustering was performed on a small subset of all the acquired
 163 images from the well-watered control plants and the different stressed groups over the entire
 164 development period. The number of clusters k was estimated by analyzing the dispersion
 165 of the within-groups sum of squares for different values of k (Sarstedt and Mooi, 2014) and
 166 was set to 12 (Figure 4). Then, the resulting cluster centroids were arranged in ascending
 167 order, based on the Euclidean norm. In the next step, the training sample size was limited
 168 to 100 spectra for each cluster, chosen relatively close to the cluster centroids. This data
 169 reduction strategy was aimed at improving the computational efficiency of SVM in both
 170 training and prediction phases (Tang et al., 2018). Then, SVM with a radial basis function
 171 kernel (Chang and Lin, 2011) was used to train the classifier and all the unlabeled spectra
 172 from the entire image collection were classified as belonging to one of the k clusters.

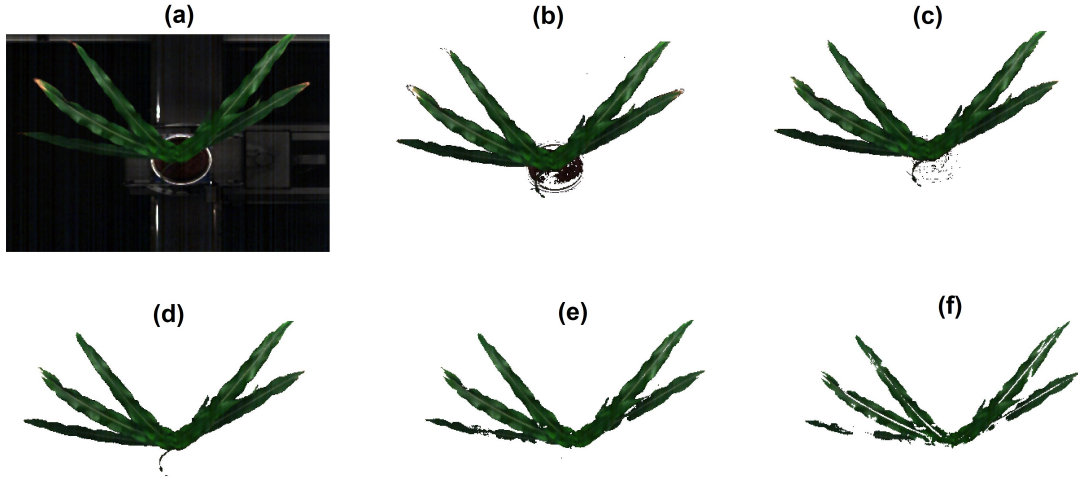


Figure 3: Segmentation of plant pixels based on NDVI threshold. Full hyperspectral image (a), segmented hyperspectral images based on NDVI threshold of 0.1 (b), 0.2 (c), 0.3 (d), 0.4 (e) and 0.5 (f).

173 Figure 5 shows an example of an obtained cluster map, in which the pixels are mapped
 174 using a false color representation in accordance with their cluster number. Based on these
 175 cluster maps, less-informative clusters were annotated and pixels from these clusters were
 176 discarded. Finally, each plant was characterized by one SNV spectrum, obtained by av-
 177 eraging the normalized spectra of all pixels belonging to the retained clusters. The entire
 178 development period of each plant is then represented as one spectral time-series.

179 2.3. Spectral similarity measure

180 To distinguish stress-related behaviour from control plant growth dynamics, a spectral
 181 similarity measure (SSM) was applied between stressed and well-watered plants. The Eu-
 182 clidean distance measure was applied to calculate the spectral distance between any two
 183 spectra $q(\lambda)$ and $r(\lambda)$:

$$ED(q, r) = \sqrt{\sum_{\lambda=1}^B (q(\lambda) - r(\lambda))^2} \quad (1)$$

184 where B is the number of bands.

185 The similarity measure allows to compare the dynamics of a plant against a reference.
 186 In this work, the reference spectrum at each day was defined as the average spectrum of all
 187 plants in the WW group of that particular day. The obtained spectral time-series represents

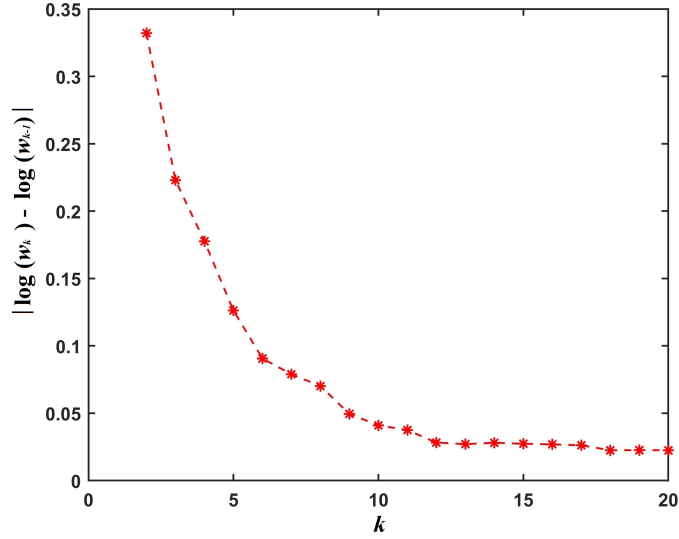


Figure 4: Choosing the number of clusters by analyzing the dispersion in the within-group sums of squares (w_k). A break point in the curve occurs at $k = 12$.

188 control plant growth and functioning dynamics. The dynamics of a control plant will be very
 189 similar to the reference time series (slightly positive since a distance is always positive), while
 190 behaviour other than the regular dynamics of the control plants will result in a significant
 191 difference with the reference time series.

192 To increase the discriminative power between stressed and control plants, a supervised
 193 band selection procedure was applied. In this work, Fisher’s statistics criterion (Grünauer
 194 and Vincze, 2015) was applied. It selects a subset of top-scoring bands with high discrimi-
 195 native power that optimise the class separability between two predefined classes (in our case
 196 well-watered versus the five groups of stressed plants). The band selection criterion was
 197 defined as:

$$\tilde{\rho}(\lambda) = \begin{cases} \rho(\lambda), & \text{if } F(\lambda) \geq T \\ 0, & \text{else} \end{cases} \quad (2)$$

198 where $\tilde{\rho}(\lambda)$ is the selected spectral band, T is a threshold value and $F(\lambda)$ is the ratio of
 199 the between-class and the within-class variance. The spectral similarity measure was then
 200 applied by only using the selected bands.

201 **3. Results and discussion**

202 In the first experiment, we validated the clustering strategy of section 2.2. To do so, we
 203 evaluated the performance of the proposed technique against the original k -means clustering
 204 algorithm. For this, a fraction (25%) of the spectral data was proportionally distributed to
 205 five test data sets, to conduct five independent experiments. The ground truth labels for
 206 this test data was obtained using the k -means clustering algorithm. Then, for each of the
 207 five experiments, 100 spectra of each cluster ($k = 12$) were randomly chosen to train the
 208 SVM. The remaining spectra acted as validation data, for which the obtained label was
 209 compared against the ground truth obtained by k -means clustering. Table 2 shows the
 210 SVM classification accuracy on this validation dataset. The overall agreement between
 211 the proposed and the k -means clustering was above 96%, confirming that the use of the
 212 supervised clustering approach was justified.

Table 2: Classification accuracy of the proposed supervised clustering approach in five independent experi-
 ments. Ground truth labeling was obtained from the k -means clustering algorithm. The processing time is
 based on the experiment running on Matlab R2018a with 4.00GHz Intel Core i7 CPU and 32.0GB system
 memory.

Data set	Number of test spectra	Match cluster between SVM and k -means (%)	Processing time (s)	
			SVM	k -means
1	2.0007×10^6	95.83	101.55	405.41
2	2.0929×10^6	96.23	105.94	439.98
3	2.3254×10^6	96.33	118.98	619.30
4	2.2473×10^6	96.32	113.82	616.38
5	2.1135×10^6	96.26	108.26	483.52
Overall performance:		96.19	109.71	512.92

213 The proposed clustering algorithm was applied to label every pixel in each individual
 214 plant and the resulting cluster map was further analyzed to filter out less-informative spectra.
 215 Figure 5 shows an example of a cluster map of a single maize plant at developmental stage

216 V13 (13 leaves developed). At this stage, the complex canopy structure may lead to non-
217 linear illumination effects, particularly due to multiple scattering. These non-linearities
218 cannot be corrected by the applied SNV normalization as that method only reduces the
219 linear effects (i.e. scaling and offset due to leaf inclination and elevation variability). From
220 visual comparison of the cluster map with the RGB image, one can notice that the lower
221 clusters (1-3) are mostly associated with regions that receive a low level of illumination
222 because they are more distant from the light source or that contain shading and partially
223 occluded leaves. Leaf edges belong to these lower clusters as well. The spectra in these
224 regions are expected to be influenced by multiple scattering and were therefore discarded
225 from further analysis.

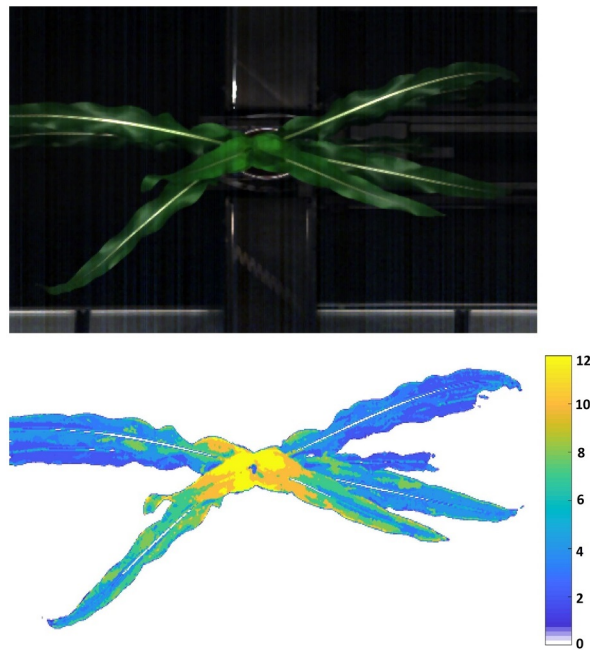


Figure 5: RGB image and cluster map from a maize plant at the V13 growing stage.

226 The next experiment was an actual experiment with well-watered control and water-
227 deficit stress treatments to monitor the growth dynamics of the plants from the six different
228 watering treatment groups, and to analyse the response to drought and recovery after re-
229 watering. The proposed method from section 2.3 was applied to obtain the spectral distance
230 of each plant from the reference spectra, during the entire experiment (53 days). The well-

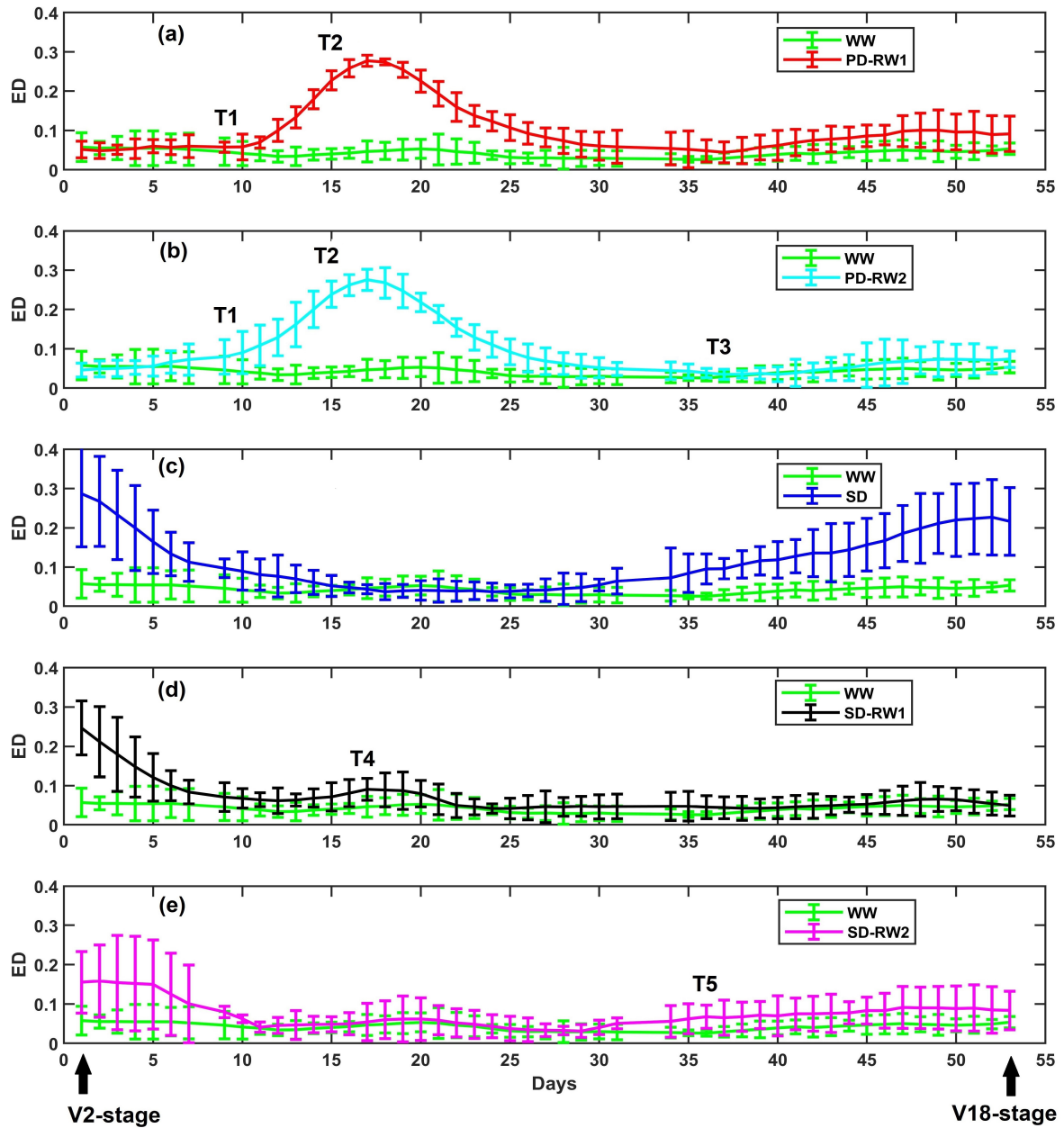


Figure 6: Evolution of the spectral distance with respect to the control group throughout the drought stress experiment for the WW control group, the PD-RW1 group (acute drought between T1 and T2), the PD-RW2 group (acute drought between T1 and T2 and re-watering to WW level at T3), the SD group and the SD-RW1 (re-watering to WW level at T4), and SD-RW2 groups (re-watering to WW level at T5). Plants grew from the V2 until the V18-stage.

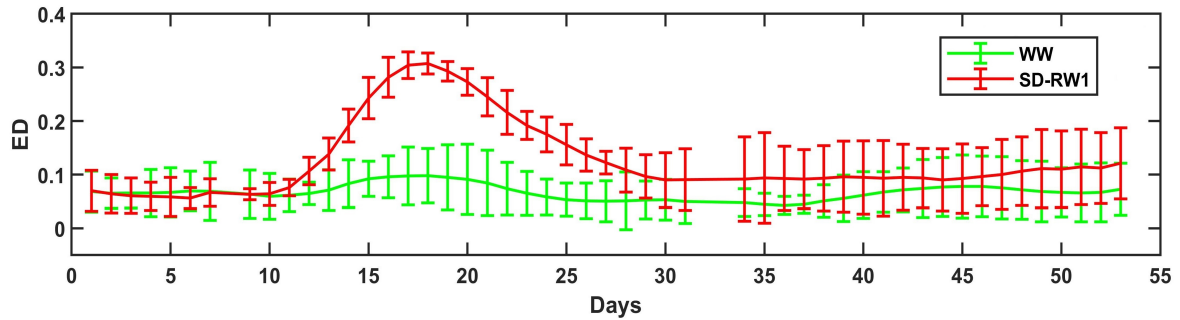


Figure 7: The obtained spectral distance when no cluster treatment was performed. The evolution plots show the comparison between plants in PD-RW1 group versus control plants throughout the drought stress experiment.

231 watered group acts as a control group. Figure 6 shows the plots for the five different stressed
 232 groups, each time compared to the plot of the WW control group. Each data point is an
 233 average over all plants of the group; standard deviations are given as well. Note that there
 234 were no measurements available on days 8, 32 and 33.

235 Figure 6(a) shows the results of the group PD-RW1 versus the WW control group.
 236 The drought stress was detected as early as the third day of the drought induction (at
 237 T1, irrigation was completely stopped). The difference with the control group gradually
 238 increased as the plants were withheld from water. At T2, 7 days after T1, the plants were
 239 watered again albeit to a lower soil water content than the well-watered treatment, after
 240 which the difference started to decrease, indicating that the plants were recovering. About
 241 15 days after re-watering, the plants seemed to have completely recovered. However, this
 242 situation did not persist until the end of the developmental period, as after day 40, the
 243 difference with the control started to grow again. Apparently, the plants initially adapted to
 244 the lower soil water content, but at a later development stage, they seemed to re-experience
 245 drought stress.

246 Figure 6(b) shows the results of the group PD-RW2 versus the control group. The water
 247 treatment of this group is identical to the one of PD-RW1 up to day 37 (T3). As expected,
 248 the behaviour is very similar to the behaviour of the PD-RW1 group. After that day, the
 249 plants were irrigated again with higher water levels equivalent to the WW treatment. From

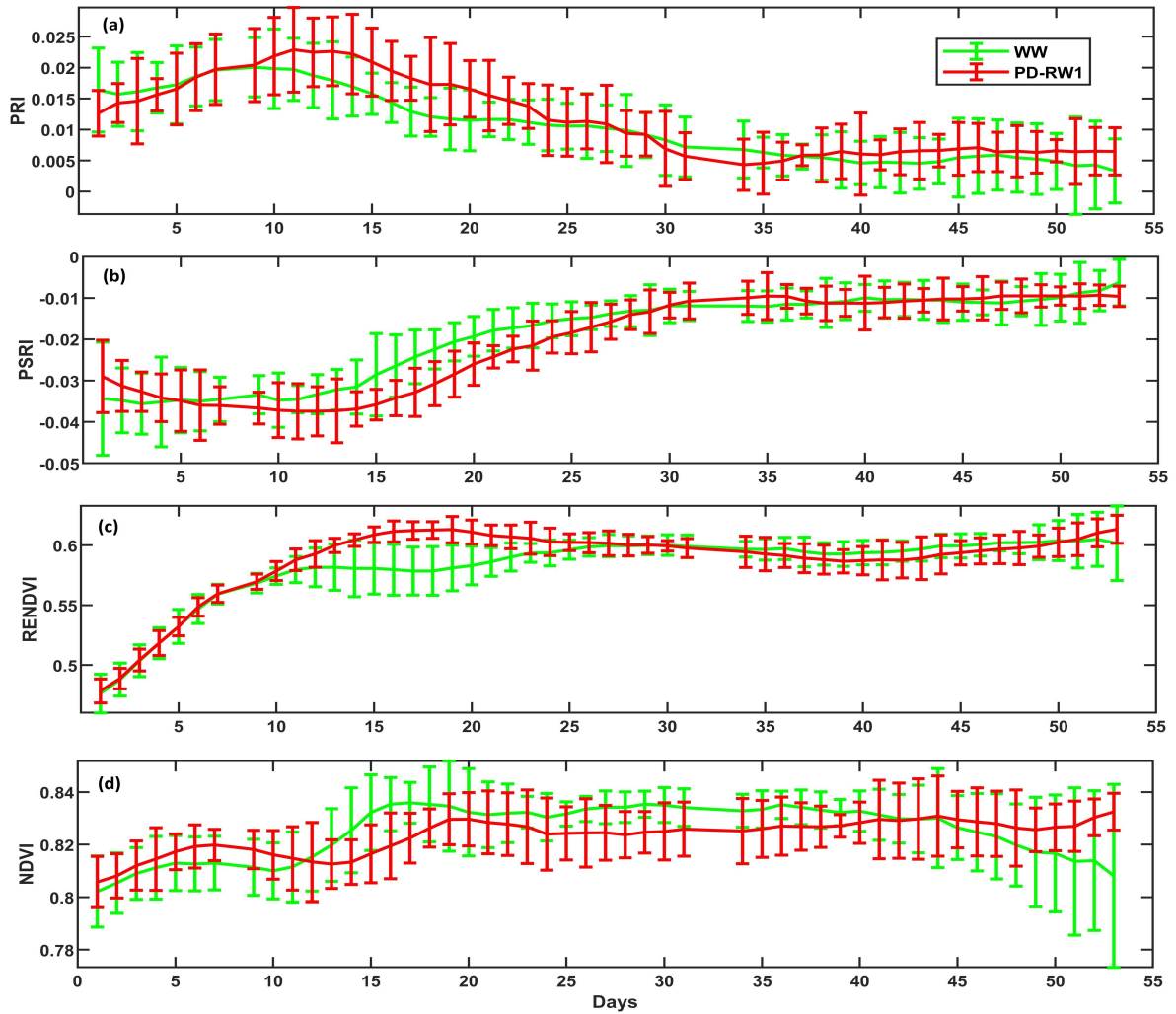


Figure 8: Evolution of spectra for the plants in PD-RW1 group versus plants in the WW group based on the calculation of vegetation indices (a) PRI (b) PSRI and (c) RENDVI (d) NDVI.

250 day 40 on (3 days after starting the WW treatment), a significant deviation from PD-RW1
 251 group was observed, as the PD-RW2 group seemed to have fully recovered from the drought
 252 stress.

253 Figure 6(c) shows the results of the group SD versus the control group. Since the irri-
 254 gation for SD plants was limited from the start (i.e. two weeks before day 1), the effect of
 255 drought stress was visible from the first day of observation. From that day on, the difference
 256 with the control group decreases monotonically until day 10, indicating that the drought

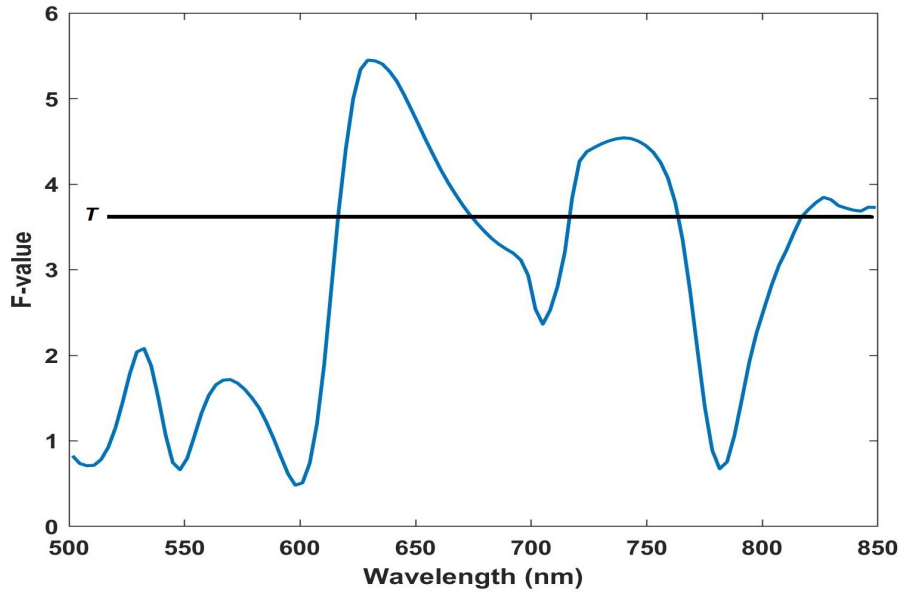


Figure 9: The F -value obtained from the band selection procedure. The threshold was set to 70% of the maximum F value.

257 plants were adapting to the water stress environment. From the literature, it is known that
 258 plants can adapt through various biological mechanisms (Xu et al., 2010; Zegada-Lizarazu
 259 and Monti, 2013; Sun et al., 2016). After this, the plants seemed to behave as WW control
 260 plants until day 35, after which the plants start to re-experience drought stress. This effect
 261 seemed to start earlier and to be more severe than for the plants in the progressive drought
 262 treatment (PD-RW1), indicating a very serious impairment in the plant development of the
 263 SD group.

264 For the remaining two groups, SD-RW1 and SD-RW2, the goal was to evaluate to what
 265 extent plants have the capacity to recover from severe drought stress when re-watering is
 266 performed. The SD-RW1 group was fully re-watered after severe drought induction, at an
 267 early vegetative state (V7), while SD-RW2 was fully re-watered at a later development stage
 268 (V12). Figures 6(d) and (e) show the results of these groups versus the control group. For
 269 the SD-RW1 group, the plant health status stabilizes shortly after re-watering (at point T4)
 270 and remains undifferent from the control group until the end of the vegetative development
 271 stage. This indicates that these plants were able to fully recover and regain their optimal

272 growth and functioning pattern. However, this was not achieved by the SD-RW2 group,
273 that deviates from the control group after the late re-watering period (T5). This indicates
274 that re-watering at a later development stage does not allow plants to entirely recover from
275 severe drought stress.

276 In the next experiment, the aim was to study the positive effect of the cluster procedure
277 on the results. For this, the same experiment on the WW and the PD-RW1 groups was
278 repeated but then without performing the clustering. As a consequence, all pixels of the
279 plants, including the ones that were influenced by nonlinear effects, were included in the
280 experiment. All other procedures, i.e. SNV normalization and band selection were performed
281 as before.

282 Figure 7 plots the evolution of the plants in the PD-RW1 group against the WW control
283 group. From this plot, it can be observed that in general, the standard deviations were
284 larger than in the original experiment. This effect was rather small at the early vegetation
285 stages, but became large during the later vegetation stages, where the canopies were large
286 and more complex, and thus the effects of multiple scattering and shading becoming more
287 serious. Because of this, during the early vegetation stage, not performing the clustering
288 had only a minor effect on the discrimination between control and drought plants. The only
289 difference that was observed was that the onset of the water stress was detected only on
290 the fourth day after the drought induction, one day later than the case where clustering
291 was applied. However, at later vegetation stages, the high standard deviations hindered
292 the distinction between healthy and drought plants, such that the re-experience of drought
293 stress after 40 days remained entirely unnoticed.

294 Many past and recent studies have applied VIs to characterize the biophysical and phys-
295 iological plant status in response to drought stress (Rumpf et al., 2010; Kim et al., 2011;
296 Amatya et al., 2012; Sun et al., 2014; Behmann et al., 2014; Gago et al., 2015). The pho-
297 tochemical reflectance index (PRI) and the normalized difference vegetation index (NDVI)
298 are the most commonly used VIs for crop water stress assessment. Other reflectance indices
299 like the red-edge normalized difference vegetation index (RENDVI) and plant senescence
300 reflectance index (PSRI) have also been used with varying results. In Sun et al. (2014), a

Table 3: The p -values of a one-way ANOVA at the 0.05 significance level for the proposed method and the four VIs. The obtained p -values are based on the comparison between plants from the WW group and the SD-RW1 group.

Early vegetative stage						Later vegetative stage					
Day	Proposed method	PRI	PSRI	RENDVI	NDVI	Day	Proposed method	PRI	PSRI	RENDVI	NDVI
1	0.7372	0.2236	0.4022	0.7630	0.3992	27	0.0005	0.3441	0.5796	0.6976	0.0645
2	0.9277	0.5799	0.5979	0.8586	0.3863	28	0.1679	0.8147	0.2396	0.3780	0.0023
3	0.2696	0.8332	0.3635	0.9205	0.9096	29	0.0625	0.0918	0.4345	0.9798	0.0080
4	0.8635	0.4295	0.8261	0.9744	0.5388	30	0.0766	0.2084	0.3618	0.8588	0.0592
5	0.5378	0.5926	0.4745	0.9652	0.3278	31	0.1401	0.3700	0.3038	0.5027	0.1399
6	0.4600	0.5100	0.3235	0.8707	0.3206	34	0.1100	0.0652	0.4076	0.6012	0.2394
7	0.2191	0.7718	0.2154	0.9692	0.0367	35	0.2523	0.9366	0.3583	0.2406	0.1635
9	0.1683	0.2129	0.6387	0.0416	0.0737	36	0.1718	0.4621	0.3819	0.4515	0.1000
10	0.2091	0.9063	0.6815	0.1186	0.2872	37	0.0486	0.5161	0.0197	0.2593	0.0392
11	0.0366	0.8479	0.0611	0.4353	0.8184	38	0.3959	0.3895	0.6715	0.2187	0.0117
12	0.0216	0.0392	0.9530	0.0776	0.8894	39	0.6940	0.7205	0.1211	0.9861	0.5397
13	0.0000	0.0619	0.1098	0.0228	0.4294	40	0.0968	0.6887	0.4539	0.3899	0.6709
14	0.0000	0.0510	0.0314	0.0211	0.0505	41	0.0161	0.0706	0.9326	0.2079	0.8077
15	0.0000	0.0937	0.1318	0.0056	0.0092	42	0.0378	0.8634	0.9499	0.1208	0.4192
16	0.0000	0.3341	0.0569	0.0034	0.0025	43	0.0466	0.7792	0.4542	0.4301	0.7397
17	0.0000	0.0112	0.0127	0.0006	0.0042	44	0.0236	0.0442	0.5086	0.4659	0.7123
18	0.0000	0.0667	0.0073	0.0005	0.3626	45	0.0452	0.4044	0.8618	0.2917	0.9515
19	0.0000	0.0252	0.0013	0.0015	0.7318	46	0.0076	0.4155	0.3545	0.2486	0.8008
20	0.0000	0.1660	0.0891	0.0015	0.9838	47	0.0258	0.4004	0.3391	0.4173	0.5864
21	0.0001	0.1221	0.0490	0.0028	0.7882	48	0.0560	0.8625	0.2016	0.6139	0.3713
22	0.0001	0.0889	0.1008	0.0130	0.5704	49	0.0101	0.8138	0.5188	0.3303	0.3720
23	0.0001	0.9523	0.0315	0.1362	0.1930	50	0.0214	0.0148	0.2856	0.8201	0.2923
24	0.0000	0.1845	0.0538	0.1999	0.2497	51	0.0383	0.5005	0.9895	0.9784	0.3237
25	0.0005	0.5216	0.1688	0.1383	0.1961	52	0.1411	0.7394	0.9408	0.6797	0.2370
26	0.0001	0.0725	0.9700	0.2241	0.2348	53	0.0730	0.2188	0.1773	0.3711	0.0913

301 significant correlation between PRI and water content was found, while in Kim et al. (2011)
302 it was shown that RENDVI and NDVI are two indices that are highly correlated with plant
303 water stress. In addition to these indices, Behmann et al. (2014) reported PSRI as a relevant
304 indicator for detecting plant stress.

305 To test the relevance of the proposed spectral analysis method, a comparison with the
306 aforementioned VIs on the drought stress experiments was performed. To calculate the VIs,
307 no SNV normalisation was applied, because VI's need to be obtained directly from reflectance
308 spectra, and because VI's take scaling effects automatically into account. However, the
309 same clustering treatment as in the proposed method was applied to account for nonlinear
310 illumination effects.

311 Figure 8 shows the plots of PRI, PSRI, RENDVI, and NDVI of the PD-RW1 versus the
312 control group. In general, deviations from the control seem to appear at the same time
313 intervals as in the proposed method (between day 10 and day 30 and from day 40 on), but
314 less clear. To quantify this, a statistical significance test was conducted using analysis of
315 variance (ANOVA). Table 3 presents the p -values obtained from the ANOVA test at 0.05
316 significance level for the proposed method and the four VIs.

317 Among the four VIs tested, RENVI was the best index for the detection of the wa-
318 ter stress. Nevertheless, when compared to the proposed method the result was far less
319 significant. None of the VIs was able to significantly determine the recovery at the later
320 development stage. Clearly, the limited amount of spectral information provided by the VIs
321 was not sufficient for a proper analysis of the drought stress and recovery after re-watering.
322 The proposed method is capable of revealing these subtle differences by making optimal use
323 of the most discriminative spectra from the entire wavelength range.

324 In the proposed method, the discrimination between control and drought-stressed plants
325 was achieved solely by determining differences in plant spectra. Such spectral character-
326 ization is referred to as non-targeted, since it reveals no direct link between the spectral
327 reflectance and specific phenotypic traits. For a possible biological interpretation, the in-
328 formation from the band selection strategy may provide useful indicators to correlate the
329 spectral variations to specific plant traits. In Figure 9, the F -score from the band selection

330 procedure is shown. The curve follows a systematic shape with several peaks of top-scoring
331 bands with high discriminative power, occurring in the 600-700 nm, 700-780 nm and 800-850
332 nm spectral regions. The position of these peaks are quite relevant when compared with the
333 wavelengths used in the calculation RENDVI and NDVI, the best two indices proposed in
334 a study of plant responses to drought by Kim et al. (2011). This specific pattern may be
335 linked to the changes in the biological properties of the plant during the stress and recovery
336 period, such as the leaf biochemical composition, the morphology of the leaf surface and
337 the internal cell structure (Linke et al., 2008). Changes in reflectance in the visible and the
338 red-edge regions are mainly related to the modification of photosynthetic pigments, while in
339 the NIR, the reflectance is influenced by light scattering of the internal properties of the cell
340 structure that is related to leaf thickness and plant dry matter (Peñuelas and Filella, 1998).

341 Another remark is that, the proposed method avoid the wavelength region in the ex-
342 tremities of the global range of spectral bands because of noise. However, previous literature
343 (Peñuelas et al., 1993; Serrano et al., 2000) suggested that spectral beyond 850 nm are also
344 useful for a direct assessment of plant stress. To test whether the information from this spec-
345 tral region can improve our earlier results, we reapplied our methodology by considering the
346 spectral range up to 1,000 nm. Figure 10 shows the F -value calculated for this wavelength
347 range. Compared to Figure 9 the systematic pattern remained similar, indicating that the
348 locations of the important information did not change. From our analysis of F -score curve,
349 the value of F -score decrease after the 850 nm region. It can also be observed that a slight
350 peak occurs around 900-950 nm water absorption region, however such peak is still less
351 dominant as compared to the spectral variation at 600-700 nm, 700-800 nm and 800-850.
352 In order to include information from bands beyond 850 nm, the threshold for F -value need
353 to be reduced, and this we expect that it may not increase the discrimination results. A
354 possible explanation is that the biological changes beyond the 850 nm wavelength region
355 could be very subtle, and because the extreme level of signal noise in this region it overlays
356 the important signature correlated to with plant traits.

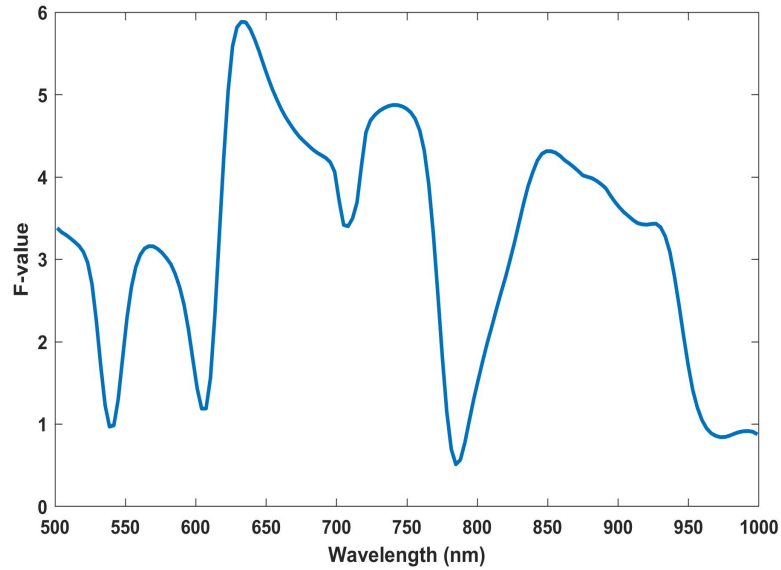


Figure 10: The F -value obtained from the band selection procedure. The threshold was set to 70% of the maximum F value.

357 4. Conclusions and future perceptive

358 In this study, it was demonstrated that HSI is a promising rapid and nondestructive
 359 technique for the detection of drought stress responses of individual plants over time. The
 360 proposed method is able to reveal drought stress and recovery from drought stress from
 361 spectral reflectance by a data-driven method that combines clustering, band selection, and
 362 a spectral similarity measure. In the experiments, the analysis method was validated in a
 363 HTPP in a study of maize plants undergoing different types of drought stress during their
 364 entire vegetative development. Experimental results showed that the method clearly dis-
 365 criminated plants under water-deficit stress from healthy plants at an early stage of stress
 366 development. The method also clearly revealed the recovery of plants after a re-watering
 367 period. This demonstrates the usefulness of HSI as a novel technology for high-throughput
 368 phenotyping studies that can boost the understanding of the genetics of drought tolerance
 369 in breeding research. It is also to be noticed that the presented method is general and not
 370 limited to drought stress, and whenever there is an interest for monitoring plant process
 371 dynamics at the plant scale, it can be applied to different types of systemic stress.

372 Further research and practical optimization are however required to fully realize its po-
373 tential for the phenotypic exploration of novel traits based upon prevailing spectra in groups
374 of genotypes, or differences in spectra between genotypes. The compensation of illumination
375 effects can be further improved by adopting more descriptive illumination models such as a
376 dichromatic reflection model (Uto and Kosugi, 2013) or digital surface models (Friman et al.,
377 2011). To attain a more accurate estimation of geometry-related parameters, the integration
378 of the 3D scene (Behmann et al., 2016) and the use of machine-learning algorithms can be
379 considered. An interesting approach to render the 3D plant model can be explored using
380 multiple viewpoints with a full frame snapshot hyperspectral camera system that captures
381 all bands simultaneously (Aasen et al., 2015). With the release of high resolution snapshot
382 hyperspectral cameras such as the Specim IQ sensor (Behmann et al., 2018), the genera-
383 tion of highly accurate 3D plant models becomes possible and interesting to be explored.
384 Another benefit of such 3D plant models is that for the data fusion capability, where the
385 physiological traits extracted from the spectral information can be fused with morphological
386 traits extracted from the 3D plant structural information. This would be the interesting
387 research direction for our future works.

388 **Acknowledgments**

389 The research presented in this paper is funded by the BAHAMAS project of the Flemish
390 research center IMEC and partly supported by the Academic Staff Training Scheme (ASTS)
391 of the Universiti Sains Malaysia and the Ministry of Higher Education of Malaysia in sup-
392 porting Mr. Mohd Shahrime Mohd Asaari for his research residency at Imec-Vision Lab
393 University of Antwerp, Belgium.

394 **References**

395 Aasen, H., Burkart, A., Bolten, A., Bareth, G., 2015. Generating 3D hyperspectral information with
396 lightweight uav snapshot cameras for vegetation monitoring: From camera calibration to quality as-
397 surance. *ISPRS Journal of Photogrammetry and Remote Sensing* 108, 245–259.

398 Amatya, S., Karkee, M., Alva, A. K., Larbi, P., Adhikari, B., 2012. Hyperspectral imaging for detecting
399 water stress in potatoes. In: ASABE Annual International Meeting, Paper number: 12-1345197.

400 Asaari, M. S. M., Mishra, P., Mertens, S., Dhondt, S., Inzé, D., Wuyts, N., Scheunders, P., 2018. Close-
401 range hyperspectral image analysis for the early detection of stress responses in individual plants in a
402 high-throughput phenotyping platform. *ISPRS Journal of Photogrammetry and Remote Sensing* 138, 121
403 – 138.

404 Behmann, J., Acebron, K., Emin, D., Bennertz, S., Matsubara, S., Thomas, S., Bohnenkamp, D., Kuska,
405 M. T., Jussila, J., Salo, H., et al., 2018. Specim IQ: Evaluation of a new, miniaturized handheld hyper-
406 spectral camera and its application for plant phenotyping and disease detection. *Sensors* 18 (2), 441.

407 Behmann, J., Mahlein, A.-K., Paulus, S., Dupuis, J., Kuhlmann, H., Oerke, E.-C., Plümer, L., 2016.
408 Generation and application of hyperspectral 3D plant models: methods and challenges. *Machine Vision*
409 *and Applications* 27 (5), 611–624.

410 Behmann, J., Steinrücken, J., Plümer, L., 2014. Detection of early plant stress responses in hyperspectral
411 images. *ISPRS Journal of Photogrammetry and Remote Sensing* 93, 98–111.

412 Chang, C.-C., Lin, C.-J., 2011. LIBSVM: A library for support vector machines. *ACM*
413 *Transactions on Intelligent Systems and Technology* 2, 27:1–27:27, Software available at
414 <http://www.csie.ntu.edu.tw/~cjlin/libsvm>.

415 Friman, O., Tolt, G., Ahlberg, J., 2011. Illumination and shadow compensation of hyperspectral images
416 using a digital surface model and non-linear least squares estimation. *Proceedings of SPIE 8180: In*
417 *Image and Signal Processing for Remote Sensing XVII*, Online: 10.1117/12.898084.

418 Gago, J., Douthe, C., Coopman, R., Gallego, P., Ribas-Carbo, M., Flexas, J., Escalona, J., Medrano, H.,
419 2015. UAVs challenge to assess water stress for sustainable agriculture. *Agricultural Water Management*
420 153, 9–19.

421 Garcia, D., 2010. Robust smoothing of gridded data in one and higher dimensions with missing values.
422 *Computational statistics & data analysis* 54 (4), 1167–1178.

423 Ge, Y., Bai, G., Stoerger, V., Schnable, J. C., 2016. Temporal dynamics of maize plant growth, water use,
424 and leaf water content using automated high throughput rgb and hyperspectral imaging. *Computers and*
425 *Electronics in Agriculture* 127, 625–632.

426 Grünauer, A., Vincze, M., 2015. Using dimension reduction to improve the classification of high-dimensional
427 data. In: 39th Annual Workshop of the Austrian Association for Pattern Recognition (OAGM 2015),
428 arXiv:1505.01065v1.

429 Heiskanen, J., Rautiainen, M., Stenberg, P., Möttus, M., Vesanto, V.-H., 2013. Sensitivity of narrowband
430 vegetation indices to boreal forest lai, reflectance seasonality and species composition. *ISPRS Journal of*
431 *Photogrammetry and Remote Sensing* 78, 1–14.

432 Ihuoma, S. O., Madramootoo, C. A., 2017. Recent advances in crop water stress detection. *Computers and*
433 *Electronics in Agriculture* 141, 267–275.

434 Jacquemoud, S., Verhoef, W., Baret, F., Bacour, C., Zarco-Tejada, P. J., Asner, G. P., François, C., Ustin,
435 S. L., 2009. Prospect+ sail models: A review of use for vegetation characterization. *Remote Sensing of*
436 *Environment* 113, S56–S66.

437 Jay, S., Bendoula, R., Hadoux, X., Féret, J.-B., Gorretta, N., 2016. A physically-based model for retriev-
438 ing foliar biochemistry and leaf orientation using close-range imaging spectroscopy. *Remote Sensing of*
439 *Environment* 177, 220–236.

440 Jay, S., Gorretta, N., Morel, J., Maupas, F., Bendoula, R., Rabatel, G., Dutartre, D., Comar, A., Baret,
441 F., 2017. Estimating leaf chlorophyll content in sugar beet canopies using millimeter-to centimeter-scale
442 reflectance imagery. *Remote Sensing of Environment* 198, 173–186.

443 Katsoulas, N., Elvanidi, A., Ferentinos, K. P., Kacira, M., Bartzanas, T., Kittas, C., 2016. Crop reflectance
444 monitoring as a tool for water stress detection in greenhouses: A review. *Biosystems Engineering* 151,
445 374–398.

446 Kim, Y., Glenn, D. M., Park, J., Ngugi, H. K., Lehman, B. L., 2011. Hyperspectral image analysis for water
447 stress detection of apple trees. *Computers and Electronics in Agriculture* 77 (2), 155–160.

448 Li, M., Cheng, Y., Zhao, H., 2004. Unlabeled data classification via support vector machines and k-means
449 clustering. In: *Proceedings of the International Conference on Computer Graphics, Imaging and Visual-*
450 *ization, CGIV*. pp. 183–186.

451 Linke, R., Richter, K., Haumann, J., Schneider, W., Weihs, P., 2008. Occurrence of repeated drought events:
452 can repetitive stress situations and recovery from drought be traced with leaf reflectance? *Periodicum*
453 *biologorum* 110 (3), 219–229.

454 Mishra, P., Asaari, M. S. M., Herrero-Langreo, A., Lohumi, S., Diezma, B., Scheunders, P., 2017. Close
455 range hyperspectral imaging of plants: A review. *Biosystems Engineering* 164 (Supplement C), 49 – 67.

456 Peñuelas, J., Filella, I., 1998. Visible and near-infrared reflectance techniques for diagnosing plant physio-
457 logical status. *Trends in Plant Science* 3 (4), 151–156.

458 Peñuelas, J., Filella, I., Biel, C., Serrano, L., Save, R., 1993. The reflectance at the 950–970 nm region as
459 an indicator of plant water status. *International journal of remote sensing* 14 (10), 1887–1905.

460 Rapaport, T., Hochberg, U., Shoshany, M., Karnieli, A., Rachmilevitch, S., 2015. Combining leaf physiology,
461 hyperspectral imaging and partial least squares-regression (pls-r) for grapevine water status assessment.
462 *ISPRS Journal of Photogrammetry and Remote Sensing* 109, 88–97.

463 Römer, C., Wahabzada, M., Ballvora, A., Pinto, F., Rossini, M., Panigada, C., Behmann, J., Léon, J.,
464 Thureau, C., Bauckhage, C., et al., 2012. Early drought stress detection in cereals: simplex volume
465 maximisation for hyperspectral image analysis. *Functional Plant Biology* 39 (11), 878–890.

466 Rumpf, T., Mahlein, A.-K., Steiner, U., Oerke, E.-C., Dehne, H.-W., Plümer, L., 2010. Early detection
467 and classification of plant diseases with support vector machines based on hyperspectral reflectance.
468 *Computers and Electronics in Agriculture* 74 (1), 91–99.

469 Sarstedt, M., Mooi, E., 2014. Cluster analysis. In: *A concise guide to market research*. Springer, pp. 273–324.

470 Serrano, L., Ustin, S. L., Roberts, D. A., Gamon, J. A., Penuelas, J., 2000. Deriving water content of
471 chaparral vegetation from aviris data. *Remote Sensing of Environment* 74 (3), 570–581.

472 Sun, C., Gao, X., Chen, X., Fu, J., Zhang, Y., 2016. Metabolic and growth responses of maize to successive
473 drought and re-watering cycles. *Agricultural Water Management* 172, 62–73.

474 Sun, C., Li, C., Zhang, C., Hao, L., Song, M., Liu, W., Zhang, Y., 2018a. Reflectance and biochemical
475 responses of maize plants to drought and re-watering cycles. *Annals of Applied Biology* 172 (3), 332–345.

476 Sun, J., Shi, S., Yang, J., Du, L., Gong, W., Chen, B., Song, S., 2018b. Analyzing the performance of
477 prospect model inversion based on different spectral information for leaf biochemical properties retrieval.
478 *ISPRS Journal of Photogrammetry and Remote Sensing* 135, 74–83.

479 Sun, P., Wahbi, S., Tsonev, T., Haworth, M., Liu, S., Centritto, M., 2014. On the use of leaf spectral indices
480 to assess water status and photosynthetic limitations in *olea europaea* l. during water-stress and recovery.
481 *PloS One* 9 (8), e105165.

482 Tang, T., Chen, S., Zhao, M., Huang, W., Luo, J., 2018. Very large-scale data classification based on k-means
483 clustering and multi-kernel SVM. *Soft Computing*, Online at: [https://doi.org/10.1007/s00500-018-3041-](https://doi.org/10.1007/s00500-018-3041-0)
484 [0](https://doi.org/10.1007/s00500-018-3041-0).

485 Uto, K., Kosugi, Y., 2013. Leaf parameter estimation based on leaf scale hyperspectral imagery. *IEEE*
486 *Journal of Selected Topics in Applied Earth Observations and Remote Sensing* 6 (2), 699–707.

487 Verrelst, J., Camps-Valls, G., Muñoz-Marí, J., Rivera, J. P., Veroustraete, F., Clevers, J. G., Moreno,
488 J., 2015. Optical remote sensing and the retrieval of terrestrial vegetation bio-geophysical properties—a
489 review. *ISPRS Journal of Photogrammetry and Remote Sensing* 108, 273–290.

490 Xu, Z., Zhou, G., Shimizu, H., 2010. Plant responses to drought and rewatering. *Plant Signaling and*
491 *Behavior* 5 (6), 649–654.

492 Zegada-Lizarazu, W., Monti, A., 2013. Photosynthetic response of sweet sorghum to drought and re-watering
493 at different growth stages. *Physiologia Plantarum* 149 (1), 56–66.